Check for updates

Received: 18 November 2021 | Revised: 13 April 2022 | Accepted: 5 May 2022

DOI: 10.1111/ijag.16584

INTERNATIONAL JOURNAL OF Applied Glass SCIENCE

SPECIAL ISSUE ARTICLE

Structure and luminescent properties of Sm/Dy-doped $Sr_2MgSi_2O_7$ glass–ceramics

Laura Fernández-Rodríguez[1] | **Rolindes Balda**[2,3] | **Joaquín Fernández**[4] | **Alicia Durán**[1] | **María Jesús Pascual**[1]

[1]Ceramics and Glass Institute (CSIC), C/ Kelsen 5, Campus de Cantoblanco, Madrid, Spain

[2]Departamento Física Aplicada, Escuela Superior de Ingeniería, Universidad del País Vasco (UPV-EHU), Bilbao, Spain

[3]Centro de Física de Materiales CFM, (UPV/EHU-CSIC), San Sebastian, Spain

[4]Donostia International Physics Center, DIPC, San Sebastian, Spain

Correspondence
M.J. Pascual, Ceramics and Glass Institute (CSIC), C/ Kelsen 5, Campus de Cantoblanco, 28049 Madrid, Spain.
Email: mpascual@icv.csic.es

Funding information
MICINN, Grant/Award Numbers: PID2020-115419GB-C-21/C-22/AEI/, 10.13039/501100011033, PID2019-107439GB-I00, PIE-CSIC 201960E016

Abstract

Sm^{3+}-doped and Sm^{3+}/Dy^{3+} codoped SiO_2–SrO–MgO glasses were prepared by conventional melt quenching and $Sr_2MgSi_2O_7$ based glass–ceramics from sintering and crystallization of the glass powders. The thermal, structural, and optical properties of the glasses and glass–ceramics were investigated as a function of the dopant concentration. The optical characterization includes the photoluminescence spectra and the lifetimes of the $^4G_{5/2}$ (Sm^{3+}) and $^4F_{9/2}$ (Dy^{3+}) excited states. In Sm^{3+} single-doped samples, the emission intensity increases up to a concentration of 0.3 mol% Sm^{3+} ions and then decreases due to nonradiative energy transfer processes. The emission spectra in the glass–ceramics show a more resolved structure and higher intensity compared to the glass samples, suggesting a different and crystalline environment for the Sm^{3+} ions. The non-radiative processes also influence the experimental decays of the glass samples which deviate from a single exponential with lifetimes decreasing as Sm^{3+} concentration increases. The emission and excitation spectra of the codoped samples do not show significant energy transfer between Sm^{3+} and Dy^{3+} ions. Different emitting colors can be obtained in the codoped glasses by changing the excitation wavelength. The studied glass–ceramics could be applied as enamels on ceramic or metallic substrates.

KEYWORDS
Dy^{3+}, glass–ceramics, luminescence, phosphors, Sm^{3+}, $Sr_2MgSi_2O_7$

1 | INTRODUCTION

Rare-earth-doped luminescent glasses and glass–ceramics have gained great attention due to their good fluorescent characteristics, high conversion efficiency, and stable physical and chemical properties.[1] In particular, phosphorescent silicate-based glass–ceramics have interesting potential applications due to the thermal stability and good physical and chemical properties of the silicate crystals. Phases such as $Ca_2MgSi_2O_7$: Eu^{2+}, Dy^{3+} [2] and $Sr_2MgSi_2O_7$: Eu^{2+}, Dy^{3+} [3] have shown good luminescent properties and long afterglow phenomena. Much research focuses on europium-doped materials with blue emission under ultraviolet light excitation for applications such

This is an open access article under the terms of the Creative Commons Attribution License, which permits use, distribution and reproduction in any medium, provided the original work is properly cited.
© 2022 The Authors. *International Journal of Applied Glass Science* published by American Ceramics Society and Wiley Periodicals LLC.

20411294, 2023, 1, Downloaded from https://ceramics.onlinelibrary.wiley.com/doi/10.1111/ijag.16584 by Universidad Del Pais Vasco, Wiley Online Library on [09/02/2023]. See the Terms and Conditions (https://onlinelibrary.wiley.com/terms-and-conditions) on Wiley Online Library for rules of use; OA articles are governed by the applicable Creative Commons License

as traffic signs, tile decoration or fluorescent lamps,[4] however, other elements such as samarium that emit red light can be very relevant for certain optical applications.[5]

Sm^{3+} ion-doped glasses have been extensively investigated by optical spectroscopy [6], for the development of orange-red phosphors because of their potential applications in color displays, plasma display panels, and solid-state lighting.[7,8] Sm^{3+} serves as one of the best activators/dopants for orange-red emission to increase the efficiency of white light emitting diode (w-LEDs).[9] Moreover, the orange-red emission is not affected by non-radiative multiphonon relaxation processes in host with high phonon energy because the large energy difference ($\approx$ 7000 cm^{-1}) between $^4G_{5/2}$ and the next lower level $^6F_{11/2}$.

Most of the research has been focused on the study of samarium-doped oxyfluoride glasses. The luminescence properties depend directly on the concentration of samarium and exceeding a certain concentration (different for each matrix) the luminescence decreases. Suhasini et al. studied [10] Sm^{3+}-doped phosphate containing fluoride glasses with molar composition of $(56-x/2)$ P_2O_5.14 K_2O.6KF.$(15-x/2)$ BaO.9Al_2O_3.xSm_2O_3, (x = 0.01–6.0 mol%.). The analysis of the decay measurements showed that the nature of the donor–acceptor interaction mechanism and the cross-relaxation between Sm^{3+} ions depend on the glass composition and the Sm^{3+} concentration. The decay curves for the $^4G_{5/2}$ level of Sm^{3+} ions at low concentration are exponential and become non-exponential for higher concentration due to the dipole–dipole cross-relaxation between Sm^{3+} ions. The lifetime of the $^4G_{5/2}$ level decreases with increasing Sm^{3+} ion concentration. Shoaib et al. [11] prepared phosphate-based oxide and oxyfluoride glasses doped with Sm^{3+} ions by the melt quenching technique. The composition of the prepared glass samples was $(66-x)$ P_2O_5.17Li_2O.17Gd_2O_3/17GdF_3:xSm_2O_3 (x = 0.05–2 mol%). They also concluded that the luminescent properties are dependent on the Sm^{3+} concentration, the luminescence increases up to 1 mol% but then decreases for higher Sm^{3+}concentration due to non-radiative energy transfer from excited Sm^{3+} ions to unexcited Sm^{3+} ions, or due to the opening of cross-relaxation channels. The emission intensity from glass with GdF_3 is higher than that of Gd_2O_3 glasses. It was concluded that lithium gadolinium phosphate glass doped with 1 mol%. Sm^{3+} ions can be a good choice for solid-state laser and orange LED applications.

Recently, Chen et al.[12] have studied borosilicate glass–ceramics containing $Na_5Y_9F_{32}$ nanocrystals and the relationship between the intensities of Dy^{3+} and Sm^{3+} ions as dopants. They prepared transparent glasses and glass–ceramics doped with Sm^{3+}, Dy^{3+}, and Sm^{3+}/Dy^{3+}, the molar compositions of the precursor glasses were 68SiO_2.8Na_2CO_3.18H_3BO_3.6NaF.9YF_3.xSm_2O_3.yDy_2O_3 (x = 0.5, 0.8, 1, 2, y = 0.5). When the glass–ceramics are excited at various wavelengths, the emission color can be tuned from yellow to white by changing the Sm^{3+} content. The Dy^{3+} emission intensity decreases with increasing Sm^{3+} concentration. The emission spectrum of the Sm^{3+}-doped samples, under an excitation wavelength of 401 nm, shows several emission bands at 563, 600, 647, and 707 nm corresponding to the transitions $^4G_{5/2} \rightarrow {}^6H_{J/2}$ (J = 5, 7, 9, 11), respectively. In the emission spectrum of the codoped glass–ceramic, under excitation at 350 nm, three emission bands at 484, 575, and 665 nm were recorded corresponding to the Dy^{3+} transitions $^4F_{9/2} \rightarrow {}^6H_{J/2}$ (J = 15, 13, 11), respectively. It can be seen that the lack of Sm^{3+} emission may be caused by the inadequate excitation wavelength of Sm^{3+} ions. The emission intensity of Dy^{3+} decreases substantially with increasing Sm^{3+} content. The energy transfer between Dy^{3+}/Sm^{3+} ions is confirmed by means of decay curves and photoluminescence (PL) spectra. The obtained results imply that transparent glass–ceramics co-doped with Dy^{3+}/Sm^{3+} could be a significant material for w-LED application.

Nevertheless, there are very few papers related to Sm^{3+}-doped silicate based glass–ceramics. In particular, Zhang et al. [13] prepared glass–ceramics based on $Sr_2MgSi_2O_7$ phase (52.55SrO.5.05MgO.37.89SiO_2.2TiO_2.2ZrO_2.0.5Sb_2O_3, wt%) doped with 0.025–0.15 wt% Sm_2O_3. The heat treatment of bulk samples was carried out at different temperatures between 980 and 1100°C for 3 h. Bands appeared at 360 nm, 374 nm, 404 nm, 417 nm, and 475 nm in the excitation spectra registered at λ_{em} = 600 nm. The emission bands appeared at 564 nm, 600 nm, and 648 nm under excitation at λ_{exc} = 404 nm. Increasing the Sm^{3+} concentration enhances the intensity of the fluorescence spectra. In the experimental concentration range (0.05–0.3 mol%), a special concentration quenching phenomenon occurred. These authors did not report lifetime measurements of the glass–ceramics.

In previous studies, $Sr_2MgSi_2O_7$: Eu^{2+}, Dy^{3+} glass–ceramics have been obtained by melt-quenching and subsequent sintering and crystallization of glass powders, where the persistent blue emission of Eu^{2+} was investigated.[3] The objective of this paper is the preparation of Sm^{3+}-doped glass and glass–ceramics based on the same composition as well as co-doped samples with Sm^{3+}–Dy^{3+}ions for the investigation of their red emission and possible energy transfer between both ions. The study of the processing of these glass–ceramics by sintering and crystallization of glass powders is relevant for their potential application for producing enamels on ceramics or metals, and their properties will be compared with those obtained by bulk crystallization. As far as we know, there are no reports on this issue for this type of material.

20411294, 2023, 1, Downloaded from https://ceramics.onlinelibrary.wiley.com/doi/10.1111/ijag.16584 by Universidad Del Pais Vasco, Wiley Online Library on [09/02/2023]. See the Terms and Conditions (https://onlinelibrary.wiley.com/terms-and-conditions) on Wiley Online Library for rules of use; OA articles are governed by the applicable Creative Commons License

The relations between the luminescent properties and the concentration of rare earth oxides will be discussed for both the original glasses and the corresponding $Sr_2MgSi_2O_7$ glass–ceramics. Sintering and crystallization processes were investigated by differential thermal analysis (DTA), hot-stage microscopy (HSM), and X-ray diffraction (XRD). The microstructure of the glass–ceramics was observed using scanning electron microscopy-cathodeluminescence (SEM-CL) and the optical characterization was completed by PL measurements.

2 | EXPERIMENTAL PROCEDURE

2.1 | Materials preparation

Glasses of the same base composition $55SiO_2$–27SrO–18MgO (mol%) doped with Sm_2O_3 (0.05, 0.1, 0.3, 0.5, 1 mol%) and co-doped with Sm_2O_3/Dy_2O_3 (0.5Sm–0.5Dy and 1Sm–0.5Dy mol%) were prepared by melt-quenching. The raw materials for the batches preparation were SiO_2 sand (Saint-Gobain, 99.6%), $SrCO_3$ (Alfa Aesar, 97.5%), MgO (PanReac, 98%), Sm_2O_3 (Alfa Aesar, > 99.9%), and Dy_2O_3 (Alfa Aesar, > 99.9%). Batches of 80 g were mixed and stirred in a Turbula mixer for 1 h to achieve homogenization. The batches were melted in a Pt/Rh crucible covered with a Pt lid in an electric furnace in air. First, the batch is calcined at 1300°C for 1 h followed by melting twice at 1550°C for 30 min. The glasses were poured into a brass mold to obtain bulk glass rods or into water to obtain frits. The letter G would be used to name the glasses and GC to name the corresponding glass–ceramics obtained from sintering and crystallization, followed by the dopant concentration (e.g., GC–0.5Sm).

The frits were milled in a Pulverisette 6 mill for two 30 min cycles, with a 5 min break, at 400 rpm. The frits were milled in acetone using agate mortar and balls and the powders were sieved below 20 μm. Cylindrical pellets (Ø = 2.5 cm) were prepared by pressing the powder into a die (32 MPa for 3 min) before firing in an electric furnace at 1100°C (heating and cooling rate 10°C/min) for 1 min in air atmosphere to obtain the corresponding glass–ceramics.

Bulk glass rods were annealed at 740°C for 30 min with a heating ramp of 5°C/min. Then, pieces of ($10 \times 8 \times 5$ mm^3) were cut with a micro-cutter and thermally treated at 1100°C for 1 min (heating and cooling rate 10°C/min) in an air atmosphere to obtain the corresponding glass–ceramics. The glass–ceramics obtained from the crystallization of bulk glass pieces will be named as GC-bulk. Only GC-bulk-0.5Sm and GC-bulk-0.5Sm–0.5Dy were prepared to compare their optical properties with those of the same glass–ceramics processed by sintering and crystallization of glass powders.

The density of glass and glass–ceramics has been measured according to the Archimedes method using distilled water.

2.2 | Thermal and structural characterization

Small samples ($12 \times 8 \times 5$ mm^3) were cut from the glass bars and analyzed by dilatometry in a Netzsch DIL 402 PC instrument at a heating rate of 5°C/min. The coefficient of thermal expansion α (CTE) was obtained from the linear fit of the dilatometric curve in the range 100–500°C; the glass transition temperature (T_g) and dilatometric softening temperature (T_d) were also determined.

The particle size distribution of the glass powders was measured with a Mastersizer 3000 using the Fraunhofer approach. The light source is a helium–neon laser emitting light with a wavelength $\lambda = 632.8$ nm onto a wet sample. The powder samples have been initially dispersed in ethanol, using an ultrasonic bath for a few minutes before the measurement.

DTA curves were recorded with an SETARAM Setsys Evolution instrument, using glass powder of particle size < 20 μm up to 1200°C with heating rate 10°C/min.

An EM 201 side-view HSM with image analysis and 1750/15 Leica electrical furnace was used to determine the sintering and flow behavior of the glass powders. Details of the equipment have been reported previously.[14,15] Measurements were conducted in air at a heating rate of 10°C/min on powder samples with particle size < 20 μm. The temperature was measured with a Pt/Rh (6/30) thermocouple placed under the alumina support and in contact with it. The changes in the area of the samples are associated with different processes and correspond to points of viscosity that were previously determined.[16]

The glass–ceramic pellets were milled and sieved to a particle size lower than 60 μm and characterized by XRD (Bruker D8 Advance) in the range 10°−70° 2θ with a step size of 0.02°, employing CuKα1 radiation ($\lambda = 1.54056$ Å).

Glass–ceramic pieces were polished with SiC paper of decreasing grain up to P4000 and a diamond suspension up to 3 μm for SEM observation and optical characterization.

SEM of the glass–ceramic samples was performed with a Hitachi S-3000N microscope equipped with a vacuum chamber. The instrument is equipped with secondary electron (SE) and backscattering electron (BSE) detectors, as well as an Oxford Instruments energy dispersive X-ray spectroscopy (EDX) analyzer, model INCAx-sight, and allows samples to be inclined at 90°. The composition of the samples was accurate within the 1 μm spot and the EDX uncertainty (~1%).

20411294, 2023, 1, Downloaded from https://ceramics.onlinelibrary.wiley.com/doi/10.1111/ijag.16584 by Universidad Del Pais Vasco, Wiley Online Library on [09/02/2023]. See the Terms and Conditions (https://onlinelibrary.wiley.com/terms-and-conditions) on Wiley Online Library for rules of use; OA articles are governed by the applicable Creative Commons License

TABLE 1 Glass transition temperature (T_g), dilatometric softening temperature (T_d) and coefficient of thermal expansion CTE (α) determined by dilatometry

Sample	T_g (°C) ± 2	T_d (°C) ± 2	$\alpha_{100\text{-}500°C}$ ($°C^{-1}$) $\pm 0.5 \times 10^{-6}$
G-undoped	722	766	9.1
G-0.05Sm	729	772	9.8
G-0.1Sm	733	770	9.6
G-0.3Sm	728	765	9.9
G-0.5Sm	739	780	9.9
G-1Sm	731	787	9.8
G-0.5Sm-0.5Dy	737	778	9.8
G-1Sm-0.5Dy	736	793	9.8

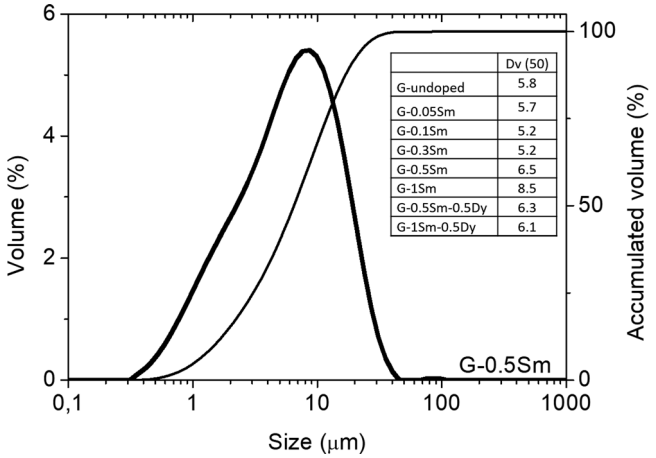

FIGURE 1 Particle size distribution for the G-0.5Sm glass powders and Dv (50) for all glass powders with different dopant concentration

SEM-CL of some selected glass–ceramic samples was performed on a Hitachi S-3000N microscope equipped with a vacuum chamber; on excitation with an electron beam of voltage 15−25 kV and a filament intensity of 100 μÅ. The emission spectra were recorded employing a fiber spectrometer with a charge-coupled device (CCD) through an optical fiber, and the corresponding luminescence photographs with an ordinary camera. The instrument is equipped with SE and BSE detectors, an EDX Quantax (model XFlash 6I30, Bruker) and a cathode-luminescence system (CHROMA-CL2 Gatan).

2.3 | Optical characterization

Conventional absorption spectra were recorded with a Cary 5000 spectrophotometer. The emission and excitation spectra, as well as temporal decays, were measured in an Edinburgh FS5 Spectrofluorometer equipped with a 150 W Xenon lamp. The emission was detected by Hamamatsu R928P photomultiplier.

3 | RESULTS AND DISCUSSION

3.1 | Thermal properties

The glass transition temperature (T_g), dilatometric softening temperature (T_d), and the CTE (α) have been obtained from dilatometric curves, these parameters are shown in Table 1. The glass transition temperature, T_g, is around 735°C and the CTE in the range 100–500°C is around $10 \pm 0.5 \times 10^{-6}$ C^{-1}. T_g and T_d do not follow a clear trend, but seem to increase with increasing Samarium concentration. The CTE is also higher in the doped glasses.

The powders obtained after milling the glass frit were sieved below 20 μm. Figure 1 shows the particle size distribution for G-0.5Sm as an example and inside the figure, a table shows the average sizes (Dv (50)) for all the powdered samples. The average particle size is between 5 and 9 μm.

Figure 2A represents the DTA results for compositions doped with different Sm concentrations. Two crystallization peaks are observed in all samples, these peaks are very well defined and more intense in the undoped and less doped samples. While in the co-doped samples both peaks are fainter, even in the co-doped sample with higher concentration both peaks are very similar with little difference in temperature. The temperature of the main crystallization peak increases when increasing samarium concentration which reflects a delay in the crystallization kinetics. The characteristic temperatures determined by DTA are around 710–730°C for the T_g, 870–890°C for T_x, and 950–980°C for T_c (Table 2).

Figure 2B shows the HSM results, the variation of the samples area (A/A_0) as a function of temperature for glass

TABLE 2 T_g, T_x, and T_c of the glasses with different Sm and Sm/Dy concentrations ($ø < 20$ μm) determined by differential thermal analysis (DTA)

Samples	T_g (°C) ± 7	T_x (°C) ±9	T_c (°C) ± 9
G-undoped	694	868	936
G-0.05Sm	712	885	960
G-0.1Sm	712	873	944
G-0.3Sm	712	886	947
G-0.5Sm	733	882	970
G-1Sm	732	893	986
G-0.5Sm-0.5Dy	732	886	968
G-1Sm-0.5Dy	734	886	1016

20411294, 2023, 1, Downloaded from https://ceramics.onlinelibrary.wiley.com/doi/10.1111/ijag.16584 by Universidad Del Pais Vasco, Wiley Online Library on [09/02/2023]. See the Terms and Conditions (https://onlinelibrary.wiley.com/terms-and-conditions) on Wiley Online Library for rules of use; OA articles are governed by the applicable Creative Commons License

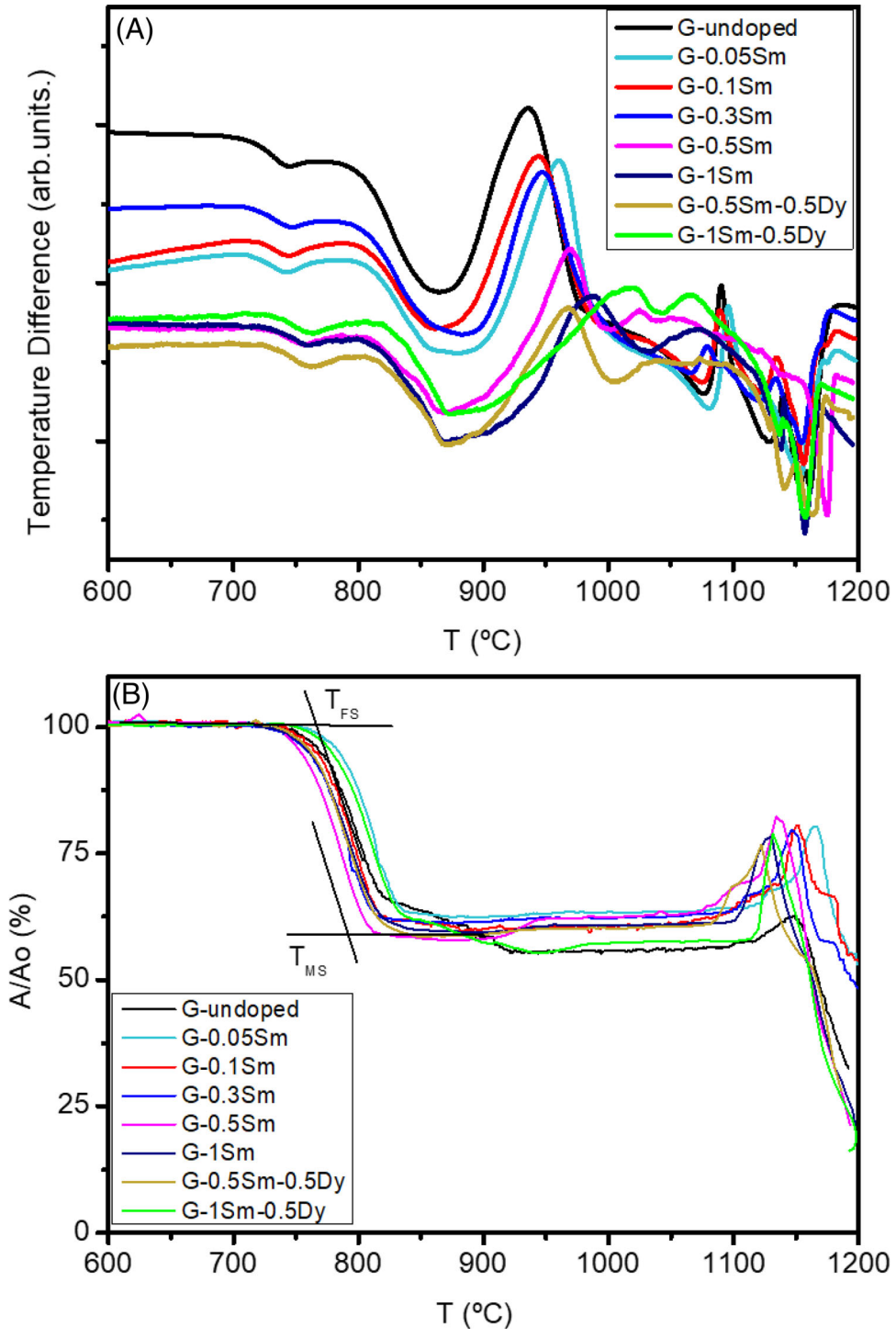

FIGURE 2 (A) Differential thermal analysis (DTA) curves of the glasses with different dopant concentrations. Heating rate: 10°C/min, (B) hot-stage microscopy (HSM) of the glass powders. Heating rate: 10°C/min

powders with different dopant concentrations; characteristic sintering and flow temperatures (first shrinkage (T_{FS}), maximum shrinkage (T_{MS}), softening (T_S), sphere (T_{Sphere}), half ball (T_{HB}), and flow (T_F)) are listed in Table 3. The maximum sintering temperatures partially overlap with the crystallization onset temperatures, which could affect densification. The softening temperature is between 850–900°C for all samples. In general, the samples become spherical around 1100°C. All samples flow from about 50°C above the sphere temperature.

The combination of the DTA and HSM results indicate that a thermal treatment of the glass powder pellets up to 1100°C can provide suitable steps of sintering, crystallization and flow, thereby enabling both glass–ceramic

20411294, 2023, 1, Downloaded from https://ceramics.onlinelibrary.wiley.com/doi/10.1111/ijag.16584 by Universidad Del Pais Vasco, Wiley Online Library on [09/02/2023]. See the Terms and Conditions (https://onlinelibrary.wiley.com/terms-and-conditions) on Wiley Online Library for rules of use; OA articles are governed by the applicable Creative Commons License

TABLE 3 Sintering and flow temperatures of the glasses from hot-stage microscopy (HSM)

Sample	T_{FS} (°C) ± 10	T_{MS} (°C) ± 10	T_S (°C) ± 10	T_{Sphere} (°C) ± 10	T_{HB} (°C) ± 10	T_F (°C) ± 3
G	761	814	860	1102	1147	1192
G-0.05Sm	783	830	861	1138	1164	1239
G-0.1Sm	756	800	888	1146	1184	1245
G-0.3Sm	750	814	890	1114	1187	1238
G-0.5Sm	748	812	890	1138	1150	1195
G-1Sm	760	816	894	1130	1145	1197
G-0.5Sm-0.5Dy	755	817	912	1126	1139	1191
G-1Sm-0.5Dy	773	883	902	1113	1151	1190

TABLE 4 Glass and glass–ceramic densities

Dopant concentration	Density ± 0.01 (g cm^{-3})		Relative density
	Glass	Glass–ceramic	
GC	3.26	2.83	0.94
GC-0.05Sm	3.30	3.22	0.98
GC-0.1Sm	3.31	3.21	0.97
GC-0.3Sm	3.31	3.12	0.94
GC-0.5Sm	3.31	2.98	0.90
GC-1Sm	3.31	3.11	0.94
GC-0.5Sm–0.5Dy	3.30	3.10	0.94
GC-1Sm–0.5Dy	3.32	3.02	0.91

in bulk or enamel form to be produced as possible final products, for example, in the ceramic tiles sector.

The densities of the glasses and glass–ceramics have been measured by the Archimedes method. The density of the glasses is around 3.3 g cm^{-3} and the corresponding glass–ceramics 3.1 g cm^{-3}. The theoretical density of the main crystalline phase, $Sr_2MgSi_2O_7$, is 3.7 g cm^{-3}. Table 4 shows all the density data of the glass and glass–ceramics that have been collected. It can therefore be concluded that there is residual porosity in all the samples, particularly in the samples with the highest Sm concentration (1 mol%).

3.2 | Structural properties

Figure 3 shows the XRD patterns of the undoped and doped glass–ceramics treated at 1100°C for 1 min. The main crystalline peaks correspond to Sr-akermanite $Sr_2MgSi_2O_7$ (ICDD: 75–1736). In the undoped glass–ceramic and also in GC-0.05Sm, GC-0.1Sm, and GC-0.3Sm (not shown) only the akermanite phase is observed. As the dopant concentration increases, a small peak corresponding to quartz

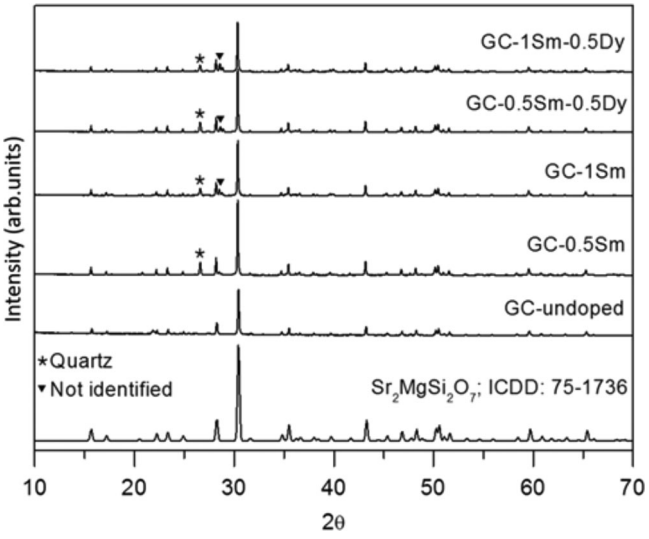

FIGURE 3 X-ray diffraction (XRD) patterns of doped glass–ceramic samples treated at 1100°C for 1 min

appears, as well as an unidentified peak that intensifies when the sample is co-doped.

The SEM images in Figure 4 show the glass–ceramic microstructures from sintering and crystallization of glass powder and how the average crystal size increases as the amount of samarium introduced into the starting glass increases.[17] Initially, the crystals of the GC-undoped measure about 0.5 μm and have spherical shape. Once samarium is added, the size increases to about 1.2 μm for the GC-0.05Sm sample up to 4.4 μm for the GC-1Sm sample. The Sm-doped samples and their corresponding Sm/Dy co-doped samples have the same crystal size. The glass–ceramic from bulk glass crystallization present a microstructure of bigger crystals and a higher amount of residual glassy phase (figures not shown).

The samarium-doped $Sr_2MgSi_2O_7$ crystals are much smaller than in the previous investigation,[3] where crystals of the same phase were obtained but doped with Eu and Eu/Dy. Therefore, it can be concluded that the type of

20411294, 2023, 1, Downloaded from https://ceramics.onlinelibrary.wiley.com/doi/10.1111/ijag.16584 by Universidad Del Pais Vasco, Wiley Online Library on [09/02/2023]. See the Terms and Conditions (https://onlinelibrary.wiley.com/terms-and-conditions) on Wiley Online Library for rules of use; OA articles are governed by the applicable Creative Commons License

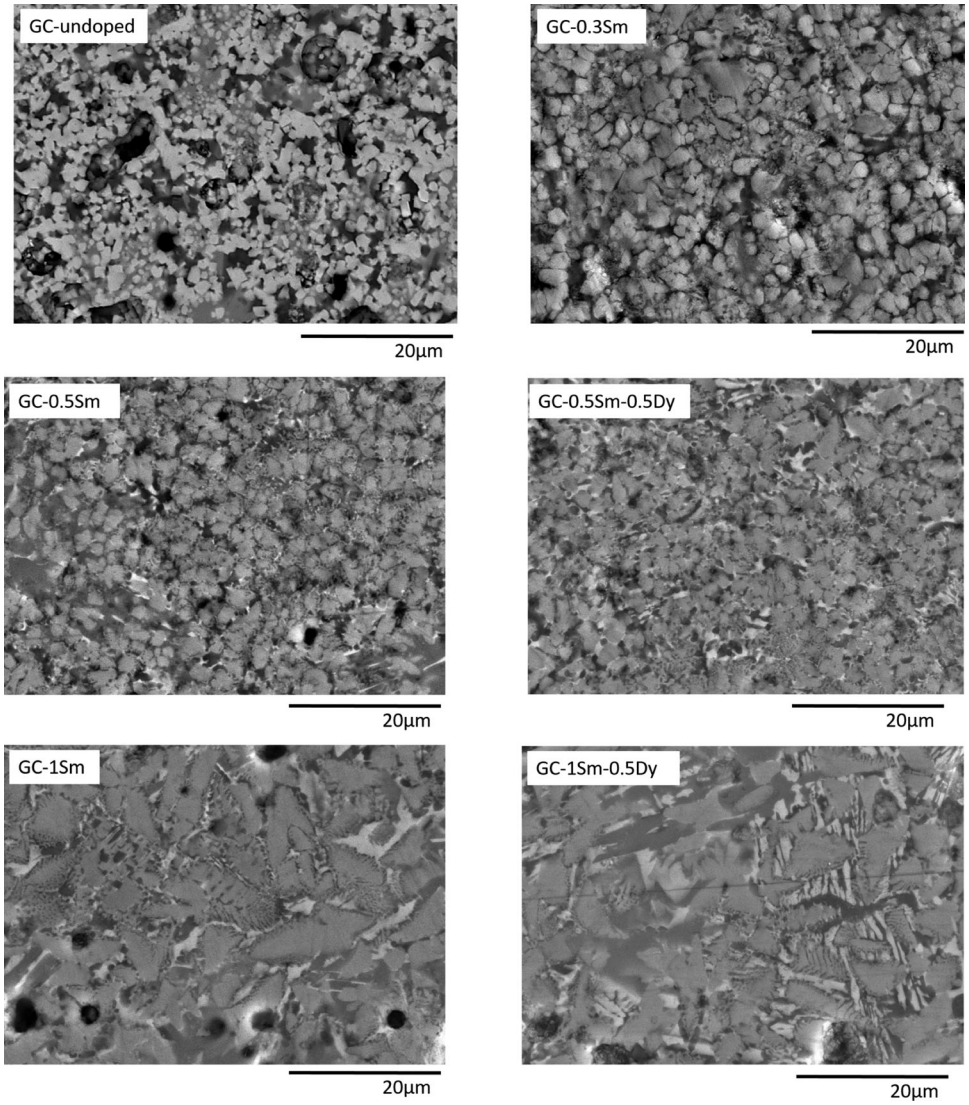

FIGURE 4 Scanning electron microscopy (SEM) of GC-undoped, GC-0.3Sm, GC-0.5Sm, GC-1Sm, GC-0.5Sm-0.5Dy, and GC-1Sm-0.5Dy samples

TABLE 5 Compositional analysis (mol%) of GC-0.5Sm–0.5Dy as determined by energy dispersive X-ray spectroscopy (EDX) corresponding to Figure 5

	Theoretical glass composition	1	2 $Sr_2MgSi_2O_7$	3	4
SiO_2	54.46	61.56	43.90	85.14	69.51
SrO	26.73	23.19	40.93	7.21	18.84
MgO	18.82	11.27	13.50	5.93	9.06
Sm_2O_3	0.50	2.34	0.81	1.08	1.39
Dy_2O_3	0.50	1.64	0.86	0.63	1.20

dopant strongly affects the nucleation and crystal growth. The samples have a high density of crystals of small size (1–5 μm).

The EDX analysis of the samples has been carried out. In particular, the analysis of the co-doped sample GC-0.5Sm–0.5Dy can be seen in Figure 5. Table 5 provides the analysis of the chemical composition of each zone measured by SEM-EDX. Point 2 corresponds to the main phase observed by XRD, $Sr_2MgSi_2O_7$, containing a small amount of samarium and dysprosium. Point 1 corresponds to some white crystals, probably from the unidentified phase, in this case the amount of samarium and dysprosium is much

20411294, 2023, 1, Downloaded from https://ceramics.onlinelibrary.wiley.com/doi/10.1111/ijag.16584 by Universidad Del Pais Vasco, Wiley Online Library on [09/02/2023]. See the Terms and Conditions (https://onlinelibrary.wiley.com/terms-and-conditions) on Wiley Online Library for rules of use; OA articles are governed by the applicable Creative Commons License

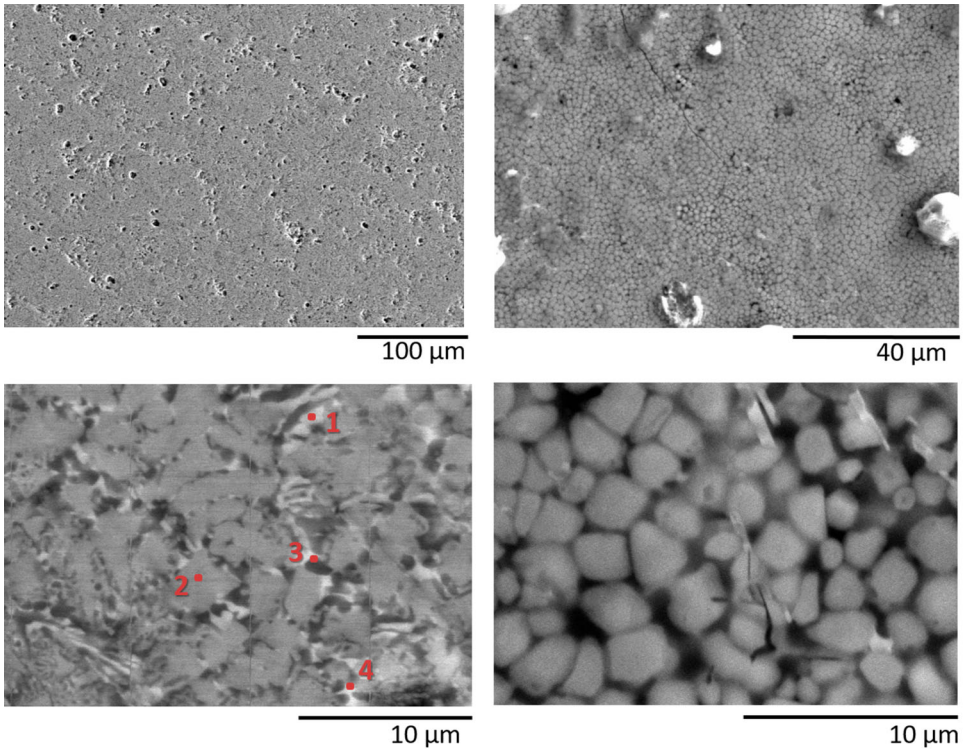

FIGURE 5 Scanning electron microscopy (SEM) images at different magnifications of GC-0.5Sm-0.5Dy

TABLE 6 Size of crystals and amount of dopant inside the crystals

	Average size of $Sr_2MgSi_2O_7$ crystals (µm)	Sm_2O_3 (EDX) (mol% in crystals)	Dy_2O_3 (EDX)(mol% in crystals)
GC-undoped	0.4	–	–
GC-0.05Sm	1.2	–	–
GC-0.1Sm	1.5	–	–
GC-0.3Sm	1.8	0.47	–
GC-0.5Sm	2.3	0.79	–
GC-1Sm	4.4	0.87	–
GC-0.5Sm–0.5Dy	2.5	0.83	0.86
GC-1Sm–0.5Dy	4.5	0.77	0.82

higher. Point 3 is a phase with a higher amount of SiO_2, so it would correspond to the quartz phase observed by XRD.

The values of the concentration of the rare earths in the table cannot be considered as an absolute value but relative to compare their distribution in the different phases. The EDX analysis does not have accuracy to determine these values which are indeed highly overestimated. Nevertheless, they indicate that there is some incorporation of Sm and Dy in the akermanite phase.

Table 6 contains an average of the crystal sizes of each GC and an average of the amount of dopant within the crystals. As mentioned above, the crystals increase in size with increasing amounts of dopant. In the Sm-doped samples the amount of dopant entering the crystals increases slightly, on the contrary in the Sm/Dy co-doped samples the amount of dopant entering the crystals seems lower, with the lowest dopant concentration inside the crystals in the GC-1Sm–0.5Dy sample.

The glass–ceramics microstructure and the crystals responsible for the emission can be observed in the panchromatic CL images. Figure 6 shows the SEM (black and white image) and panchromatic (red) images corresponding to the same area of the pellet compared at 50 µm

20411294, 2023, 1, Downloaded from https://ceramics.onlinelibrary.wiley.com/doi/10.1111/ijag.16584 by Universidad Del Pais Vasco, Wiley Online Library on [09/02/2023]. See the Terms and Conditions (https://onlinelibrary.wiley.com/terms-and-conditions) on Wiley Online Library for rules of use; OA articles are governed by the applicable Creative Commons License

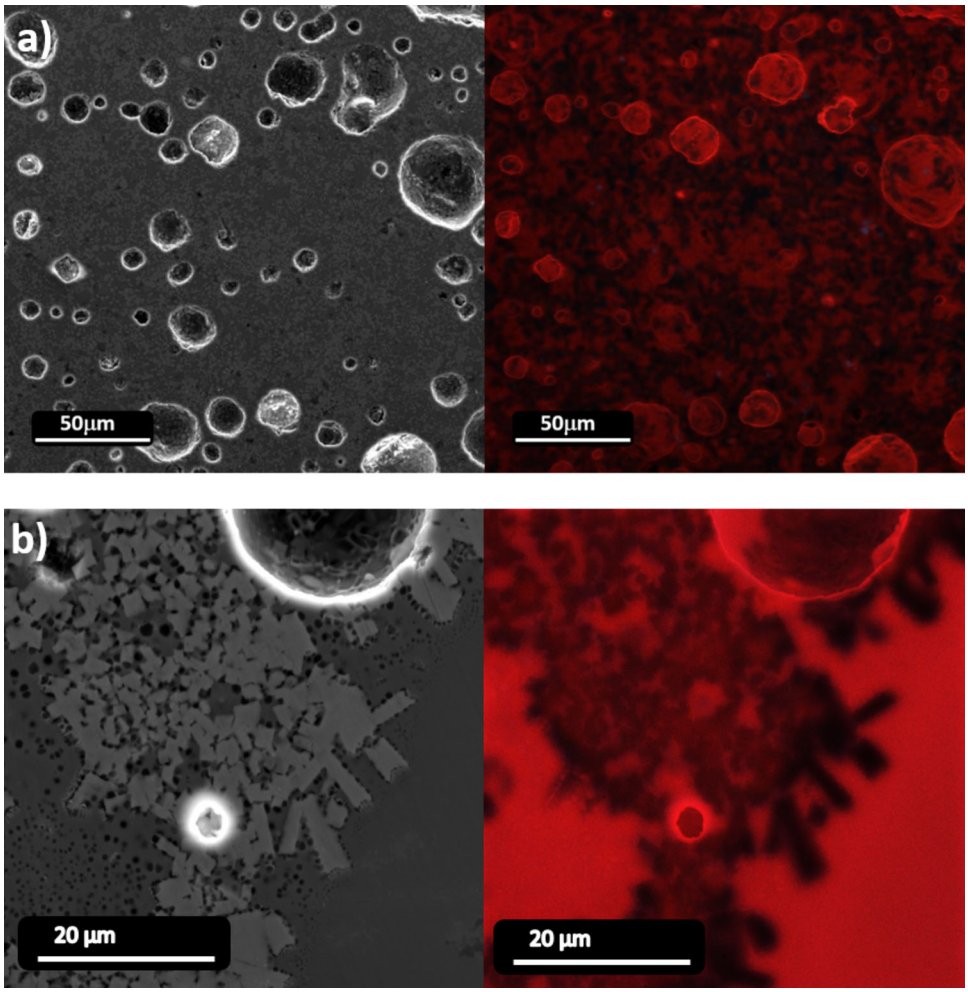

FIGURE 6 Scanning electron microscopy (SEM) and SEM-CL of GC-0.3Sm at (A) low and (B) high magnification

and 20 µm for GC-0.3Sm. Figure 6A (low magnification) shows the central surface of the polished sample, where a very homogeneous red emission is observed. Figure 6B (higher magnification) shows an area with high amount of residual glass matrix where the more intense red emission clearly comes from.

The crystallization mechanism of these glasses is preferentially superficial and crystallization takes place from the surface to the interior of the glass piece up to complete crystallization. Hence, sintering of glass powders is a good option to obtain a final more homogeneous bulk crystallization, and with a higher degree of crystallization. GC-Bulk-0.5Sm and GC-0.5Sm–0.5Dy were prepared and characterized for comparison purpose. The main crystallization phase is the same $Sr_2MgSi_2O_7$ for both types of processing. The microstructure of glass–ceramic from bulk glass crystallization (not shown) is much less crystallized (more residual glassy phase) and the crystals are larger. Nevertheless, in relation to the optical properties we will show in the next section that they offer similar luminescent characteristics.

3.3 | Optical properties

3.3.1 | Absorption spectra

Figure 7 displays the absorption coefficient for the glasses doped with 0.5 and 1 mol% Sm_2O_3 in the 320 −1800 nm spectral range. The spectra show the transitions originated from the $^6H_{5/2}$ ground state to the different excited states of Sm^{3+}. In the UV–VIS region, the spectra present the characteristics $^6H_{5/2} \rightarrow {}^4H_{9/2}$, $^4D_{3/2}$, $^6P_{7/2}$, $^6P_{3/2}$, $^6P_{5/2}$, $^4G_{9/2}$, $^4I_{13/2}$, $^4M_{15/2}$, and $^4I_{11/2}$ absorptions bands. The $^6H_{5/2} \rightarrow {}^4F_{3/2}$ and $^6H_{5/2} \rightarrow {}^4G_{5/2}$ at around 528 and 556 nm respectively are not clearly observed. The absorption bands in the near-infrared are assigned to the spin allowed ($\Delta S = 0$) transitions $^6H_{5/2} \rightarrow {}^6F_{11/2}$, $^6F_{9/2}$, $^6F_{7/2}$, $^6F_{5/2}$, $^6F_{3/2}$, $^6H_{15/2}$, and $^6F_{1/2}$ which are more intense than those in the UV–VIS region. Similar absorption spectra are obtained for all single-doped glass samples except for the band intensities which depend on Sm_2O_3 concentration. Due to the partial spectral overlapping of the Sm^{3+} and Dy^{3+} absorption bands, no significant differences

20411294, 2023, 1, Downloaded from https://ceramics.onlinelibrary.wiley.com/doi/10.1111/ijag.16584 by Universidad Del Pais Vasco, Wiley Online Library on [09/02/2023]. See the Terms and Conditions (https://onlinelibrary.wiley.com/terms-and-conditions) on Wiley Online Library for rules of use; OA articles are governed by the applicable Creative Commons License

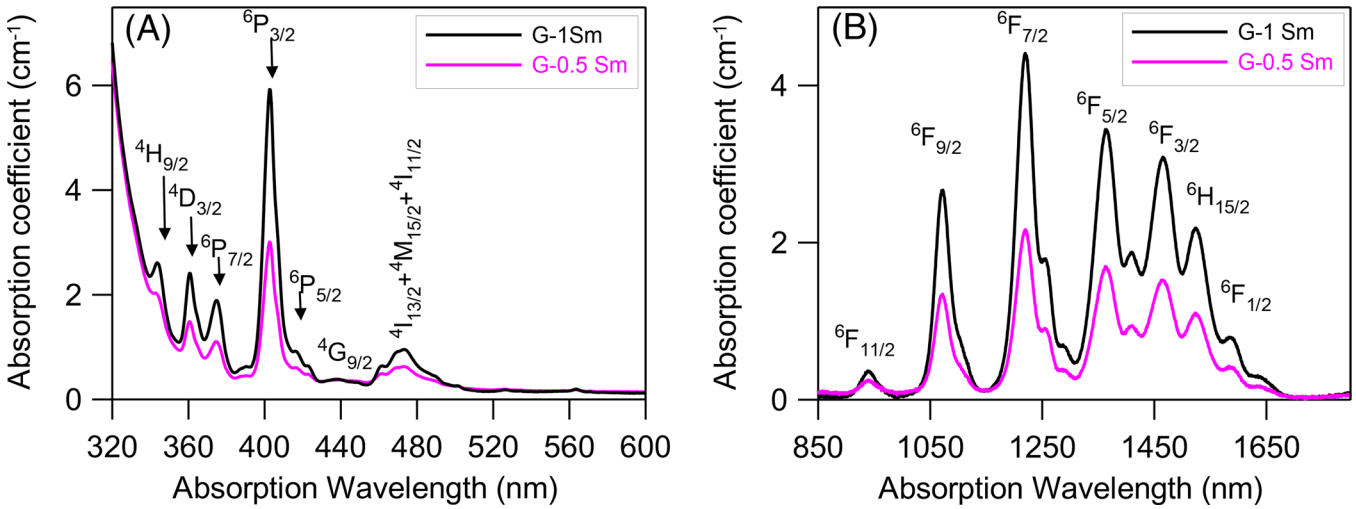

FIGURE 7 Room temperature absorption spectra for the G-0.5Sm and G-1Sm glasses in (A) UV–VIS and (B) Near infrared (NIR) regions

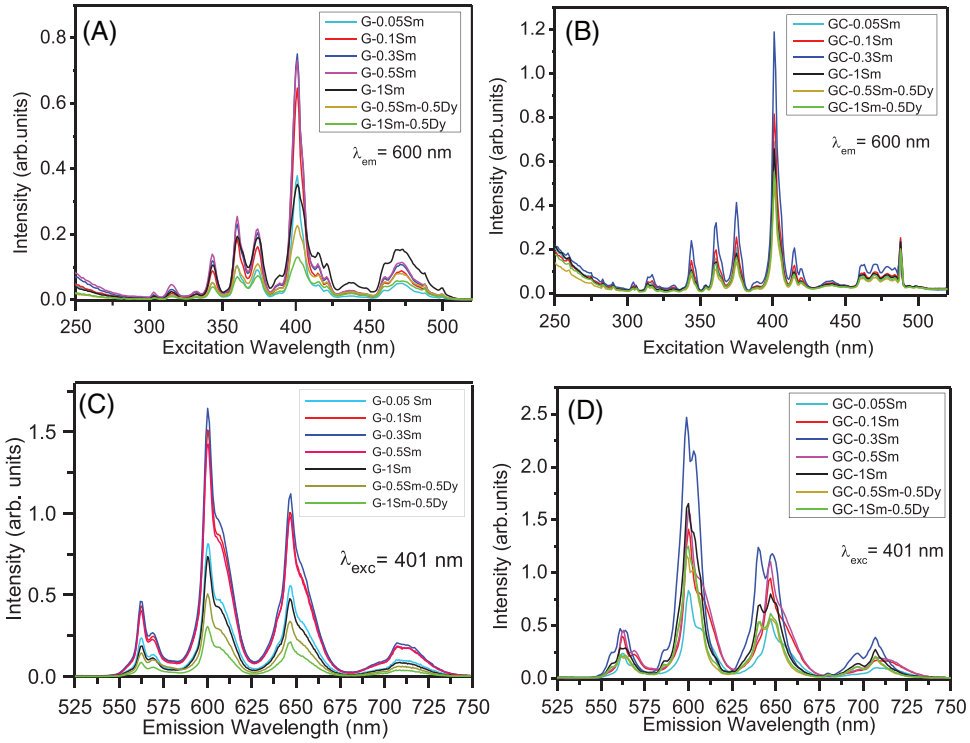

FIGURE 8 Room temperature excitation spectra obtained by collecting the luminescence at 600 nm for the (A) glass and (B) GC samples. Emission spectra obtained under 401 nm excitation in the (C) glass and (D) GC samples

were observed in the absorption spectra of the codoped samples.

3.3.2 | Excitation and emission spectra

Figure 8A,B shows the room temperature excitation spectra recorded by monitoring the $^4G_{5/2} \rightarrow {}^6H_{7/2}$ red emission of Sm^{3+} at 600 nm for the glass and glass–ceramic samples in the 250–525 nm range. In all cases, the most intense band of Sm^{3+} excitation is observed at 401 nm, so the emission spectra were obtained by exciting at that wavelength.

The room temperature emission spectra of the glass and glass–ceramic samples obtained after excitation at 401 nm in the 525–750 nm range are displayed in Figure 8C,D. The spectra of the glass samples are characterized by

20411294, 2023, 1, Downloaded from https://ceramics.onlinelibrary.wiley.com/doi/10.1111/ijag.16584 by Universidad Del Pais Vasco, Wiley Online Library on [09/02/2023]. See the Terms and Conditions (https://onlinelibrary.wiley.com/terms-and-conditions) on Wiley Online Library for rules of use; OA articles are governed by the applicable Creative Commons License

the four bands attributed to the $^4G_{5/2} \rightarrow {}^6H_{5/2}$ (562 nm), $^4G_{5/2} \rightarrow {}^6H_{7/2}$ (600 nm), $^4G_{5/2} \rightarrow {}^6H_{9/2}$ (647 nm), and $^4G_{5/2} \rightarrow {}^6H_{11/2}$ (711 nm) transitions. The emission peaks remain unchanged for all Sm^{3+} concentrations, whereas the emission intensity increases with concentration up to 0.3 mol% and then decreases due to concentration quenching. The most intense emission corresponds to $^4G_{5/2} \rightarrow {}^6H_{7/2}$ transition followed by $^4G_{5/2} \rightarrow {}^6H_{9/2}$ one. The $^4G_{5/2} \rightarrow {}^6H_{9/2,11/2}$ transitions follow the selection rule $\Delta J \leq 6$ and are electric dipole (ED), whereas the transitions $^4G_{5/2} \rightarrow {}^6H_{5/2}$ ($\Delta J = 0$) is magnetic dipole (MD) and the transition $^4G_{5/2} \rightarrow {}^6H_{7/2}$ ($\Delta J = \pm 1$) has both ED and MD character [18]. The ratio of the emission intensity of ED and MD transitions is a measure of how close is the rare-earth site to be centrosymmetric. The intensity of the ED emission transition $^4G_{5/2} \rightarrow {}^6H_{9/2}$ at 647 nm is higher than the MD transition $^4G_{5/2} \rightarrow {}^6H_{5/2}$ at 562 nm, being the $^4G_{5/2} \rightarrow {}^6H_{9/2}/{}^4G_{5/2} \rightarrow {}^6H_{5/2}$ intensity ratio around 3.2 for all glass samples which indicates asymmetric sites for the Sm^{3+} ions.[19] As can be seen in Figure 8C, the presence of Dy^{3+} ions in the codoped samples leads to a reduction of the Sm^{3+} emission intensity if compared with the single doped ones which could indicate the presence of Sm^{3+}–Dy^{3+} energy transfer. However, as we will see below, the evidences of energy transfer are scarce.

The excitation and emission spectra in the glass–ceramic samples displayed in Figure 8B,D show a more resolved structure and a higher intensity compared to the glass samples which suggest a different environment for Sm^{3+} ions. As in the glass samples, the dominant emission corresponds to the $^4G_{5/2} \rightarrow {}^6H_{7/2}$ transition and the $^4G_{5/2} \rightarrow {}^6H_{9/2}/{}^4G_{5/2} \rightarrow {}^6H_{5/2}$ intensity ratio is around 3.2 for all concentrations.

As we have seen in Figure 8C,D under 401 nm excitation the codoped samples exhibit the Sm^{3+} emissions from $^4G_{5/2}$ level without the presence of Dy^{3+} emissions. At this wavelength, we mainly excite Sm^{3+} ions. This is clear from the observation of the excitation spectra obtained by collecting the luminescence at 574 nm corresponding to the $^4F_{9/2} \rightarrow {}^6H_{13/2}$ (Dy^{3+}) and at 600 nm ($^4G_{5/2} \rightarrow {}^6H_{7/2}$, Sm^{3+}). As an example, Figure 9 shows for comparison the excitation spectra of the codoped glass sample with 0.5 mol% Sm_2O_3–0.5%Dy_2O_3 obtained by collecting the luminescence at 600 nm (Sm^{3+}) and 574 nm (Dy^{3+}). As can be seen, the spectra show partial overlapping of some bands. In both codoped samples, the excitation spectra have the same profile.

To check the possibility of Dy^{3+}–Sm^{3+} energy transfer, we have excited the codoped samples at 348 nm in the $^6H_{15/2} \rightarrow {}^6P_{7/2}$ (Dy^{3+}) transition. Figure 10A displays the spectrum corresponding to the glass sample codoped with 0.5 mol% Sm_2O_3–0.5 mol% Dy_2O_3.The spectrum presents

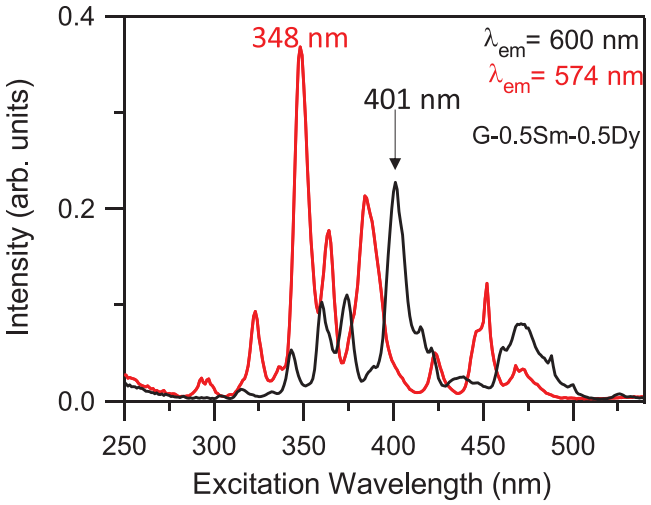

FIGURE 9 Room temperature excitation spectra for the G-0.5Sm–0.5Dy sample obtained by collecting the luminescence at 600 nm (Sm^{3+}) (black) and 574 nm (Dy^{3+}) (red)

three bands at around 484 nm, 574 nm, and 666 nm which can be ascribed to the $^4F_{9/2} \rightarrow {}^6H_{15/2}$, $^4F_{9/2} \rightarrow {}^6H_{13/2}$, and $^4F_{9/2} \rightarrow {}^6H_{11/2}$ transitions of Dy^{3+}, respectively. The blue emission ($^4F_{9/2} \rightarrow {}^6H_{15/2}$) is MD, whereas the yellow ($^4F_{9/2} \rightarrow {}^6H_{13/2}$) is a hypersensitive ED, which is strongly affected by the crystal-field environment, and the red $^4F_{9/2} \rightarrow {}^6H_{11/2}$ one is also ED. The intensity ratio of the yellow to blue emissions is around 4.2 in both codoped glass samples which indicates that Dy^{3+} ions are located in a low symmetry site without inversion center.[19]

In addition to the Dy^{3+} emissions, the spectrum shows a very weak peak at 600 nm corresponding to the $^4G_{5/2} \rightarrow {}^6H_{7/2}$ emission of Sm^{3+} which could indicate the presence of a weak Dy^{3+}–Sm^{3+} energy transfer. However, due to the spectral overlapping of the excitation spectra of the Sm^{3+} and Dy^{3+} ions we cannot confirm this energy transfer. In fact, after excitation at 348 nm, which is a characteristic excitation band of the Dy^{3+} ions, the single-doped glass with only Sm^{3+} ions emits only the characteristic Sm^{3+}emission bands. Regarding the possibility of Sm^{3+}–Dy^{3+} energy transfer after 401 nm excitation, which corresponds to the main absorption transition of Sm^{3+}, the emission spectra of the codoped samples show in addition to the $^4G_{5/2} \rightarrow {}^6H_{5/2}$ (562 nm), $^4G_{5/2} \rightarrow {}^6H_{7/2}$ (600 nm), $^4G_{5/2} \rightarrow {}^6H_{9/2}$ (647 nm), and $^4G_{5/2} \rightarrow {}^6H_{11/2}$ (711 nm) Sm^{3+} emissions, a weak $^4F_{9/2} \rightarrow {}^6H_{15/2}$ blue emission of Dy^{3+} ions. As an example, Figure 10B shows the spectrum for the G-0.5Sm–0.5Dy codoped sample. However, the intensity of the weak blue emission can be attributed to the simultaneous excitation of both ions more than to energy transfer. It is worthy to mention that in the excitation spectra monitored at 600 nm (Sm^{3+}), only the f–f transitions of Sm^{3+} are observed and the same occurs for the spectra monitored

20411294, 2023, 1, Downloaded from https://ceramics.onlinelibrary.wiley.com/doi/10.1111/ijag.16584 by Universidad Del Pais Vasco, Wiley Online Library on [09/02/2023]. See the Terms and Conditions (https://onlinelibrary.wiley.com/terms-and-conditions) on Wiley Online Library for rules of use; OA articles are governed by the applicable Creative Commons License

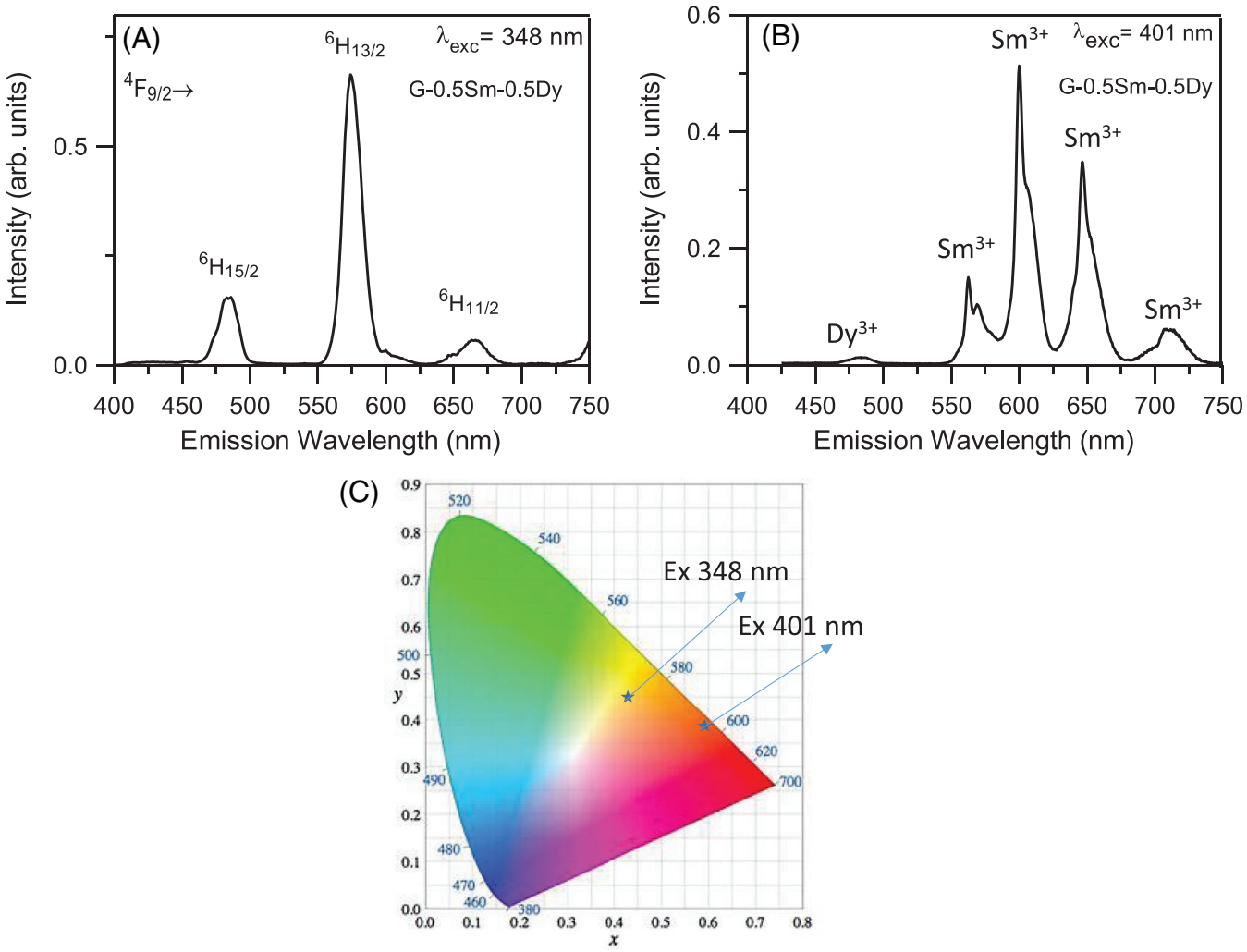

FIGURE 10 Room temperature emission spectra in the G-0.5Sm–0.5Dy sample obtained (A) under 348 nm (Dy^{3+}) excitation and (B) under 401 nm (Sm^{3+}) excitation. (C) CIE chromaticity coordinates for the two different excitation wavelengths

at 574 nm (Dy^{3+}), where only the Dy^{3+} ions transitions appear. If energy transfer had occurred between Sm^{3+}–Dy^{3+} pair, the excitation spectra should include the peaks of both ions. Therefore, the excitation and emissions spectra suggest the absence of any significant energy transfer between both ions. This behavior has also been observed in other Sm^{3+}–Dy^{3+} codoped systems.[20,21]

The calculated chromaticity coordinates calculated for two excitation wavelengths 348 and 401 nm are illustrated in Figure 10C. The points represent the CIE (Commission Internationale de l'Elcairage) coordinates. The chromaticity coordinates move from yellow ($x = 0.4324$, $y = 0.4485$) to red ($x = 0.5799$, $y = 0.3868$) when the excitation wavelength changes from 348 nm (Dy^{3+}) to 401 nm (Sm^{3+}) which means that the output color can be tuned by controlling the excitation wavelength.

The emission of the GC samples after excitation of Dy^{3+} ions at 348 nm is too weak to be accurately measured.

The emission and excitation spectra of the GC samples obtained by the thermal treatment of the as-quenched glass do not show any significant difference with those of GCs obtained by sintering and crystallization of glass powders. As an example, Figure 11 displays the emission spectra of the GC-0.5Sm–0.5Dy samples obtained by sintering and crystallization of glass powders and by bulk crystallization.

3.3.3 | Lifetimes

The decays of the $^4G_{5/2}$ level were obtained for all samples by exciting at 401 nm and collecting the luminescence at the maximum of the $^4G_{5/2} \rightarrow {}^6H_{7/2}$ emission. In the case of the single-doped glass samples, the decay for the lowest Sm^{3+} concentration (0.05%) can be described by a single exponential function to a good approximation

20411294, 2023, 1, Downloaded from https://ceramics.onlinelibrary.wiley.com/doi/10.1111/ijag.16584 by Universidad Del Pais Vasco, Wiley Online Library on [09/02/2023]. See the Terms and Conditions (https://onlinelibrary.wiley.com/terms-and-conditions) on Wiley Online Library for rules of use; OA articles are governed by the applicable Creative Commons License

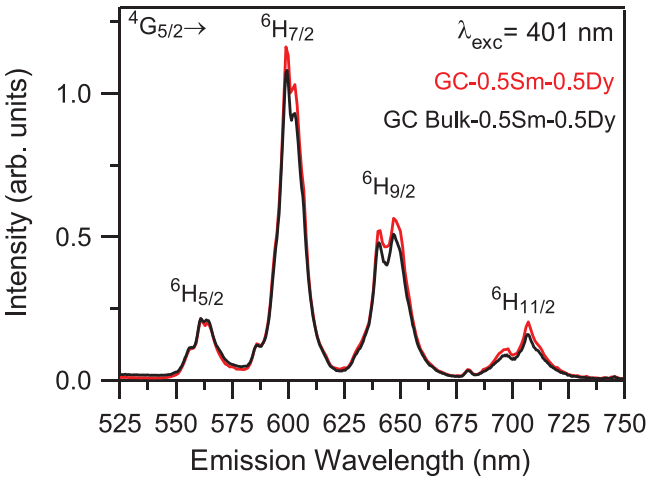

FIGURE 11 Room temperature emission spectra in the glass–ceramic samples codoped with 0.5 mol% Sm_2O_3–0.5 mol% Dy_2O_3 processes by sintering and crystallization of glass powders (red line) and from bulk crystallization (black line) under 401 nm excitation

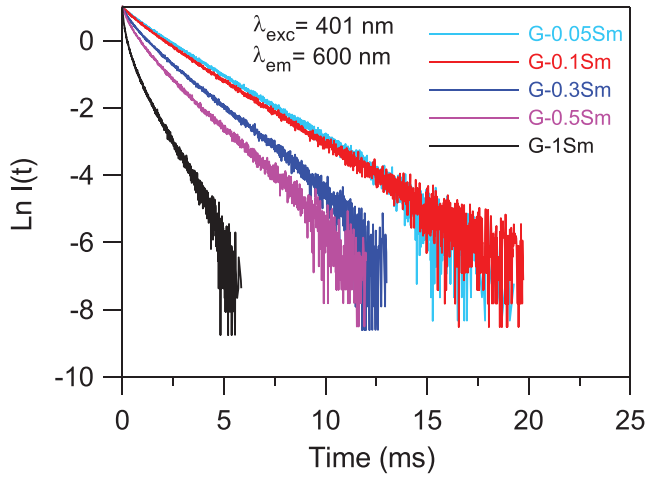

FIGURE 12 Semilogarithmic plot of the fluorescence decays of the $^4G_{5/2}$ level obtained under 401 nm excitation for the glass samples with different Sm_2O_3 contain

with a lifetime of 2.4 ms. As Sm^{3+} concentration increases, the decays deviate from a single exponential and the lifetimes decrease to 0.5 ms for the sample doped with 1 mol% Sm_2O_3 (Figure 12). In the glass–ceramic samples, the decays slightly deviate from a single exponential but the shortening of the lifetimes is much less pronounced than in the glass samples. The lifetime decreases from 2.2 ms to 1.9 as concentration increases up to 0.3 mol% and then increases up to 2.1 and 2.2 ms for the samples with 0.5 and 1 mol% Sm_2O_3, respectively. This could indicate that the Sm^{3+} concentration in these samples is less than the nominal one. Table 7 shows the lifetime values for the Sm_2O_3 single-doped samples. The lifetime values in Table 7 for the non-exponential decays correspond to the average lifetime, calculated by:

$\langle\tau\rangle = \frac{\int_0^\infty tI(t)dt}{\int_0^\infty I(t)dt}$, where $I(t)$ represents the luminescence intensity at time t corrected for the background.

TABLE 7 Lifetime values obtained under excitation at 401 nm collecting the luminescence at the maximum of the $^4G_{5/2} \rightarrow {}^6H_{7/2}$ emission for the glass and glass–ceramic samples doped with different Sm_2O_3 concentrations

Sample	Lifetime (ms)
G-0.05Sm	2.4
G-0.1Sm	2.2
G-0.3Sm	1.5
G-0.5Sm	1.1
G-1Sm	0.5
GC-0.05Sm	2.2
GC-0.1Sm	2.1
GC-0.3Sm	1.9
GC-0.5Sm	2.1
GC-1Sm	2.2

The shortening of the lifetimes and the deviation from a single exponential function are characteristics of the existence of concentration quenching mechanism in the lifetime of $^4G_{5/2}$ level as concentration increases.

The experimental decay time of the $^4G_{5/2}$ level in the single-doped samples should be governed by a sum of probabilities for radiative and non-radiative processes. The nonradiative processes include nonradiative multiphonon relaxation and energy transfer through cross-relaxation, and quenching induced by impurities. Nonradiative decay by multiphonon relaxation is expected to be small because the large energy difference between $^4G_{5/2}$ and the next lower level $^6F_{11/2}$ which is around 7000 cm^{-1}. Therefore, the reduction of the lifetime as concentration increases may be mainly due to energy transfer processes via cross-relaxation ($^4G_{5/2}$;$^6H_{5/2}$) → ($^6F_{5/2}$; $^6F_{11/2}$), ($^4G_{5/2}$;$^6H_{5/2}$) → ($^6F_{7/2}$; $^6F_{9/2}$), ($^4G_{5/2}$; $^6H_{5/2}$) → ($^6F_{9/2}$; $^6F_{7/2}$), and ($^4G_{5/2}$;$^6H_{5/2}$) → ($^6F_{11/2}$; $^6F_{5/2}$).[22]

In the case of the codoped glass samples, the experimental decays of the $^4G_{5/2}$ level, obtained under excitation at 401 nm collecting the luminescence at 600 nm, show an increase of the nonexponential behavior together with a shortening of the lifetime as compared with the single-doped samples. The lifetime decreases from 1.1 ms in the glass sample doped with 0.5 mol% Sm_2O_3 to 0.47 ms and 0.21 ms in the codoped samples with 0.5 and 1 mol% Dy_2O_3, respectively. As an example, Figure 13A shows the experimental decays of the $^4G_{5/2}$ level in the 0.5 mol% Sm_2O_3 single-doped sample and in the codoped sample with 0.5 mol% Dy_2O_3. This behavior could be attributed to the additional probability of relaxation by nonradiative

20411294, 2023, 1, Downloaded from https://ceramics.onlinelibrary.wiley.com/doi/10.1111/ijag.16584 by Universidad Del Pais Vasco, Wiley Online Library on [09/02/2023]. See the Terms and Conditions (https://onlinelibrary.wiley.com/terms-and-conditions) on Wiley Online Library for rules of use; OA articles are governed by the applicable Creative Commons License

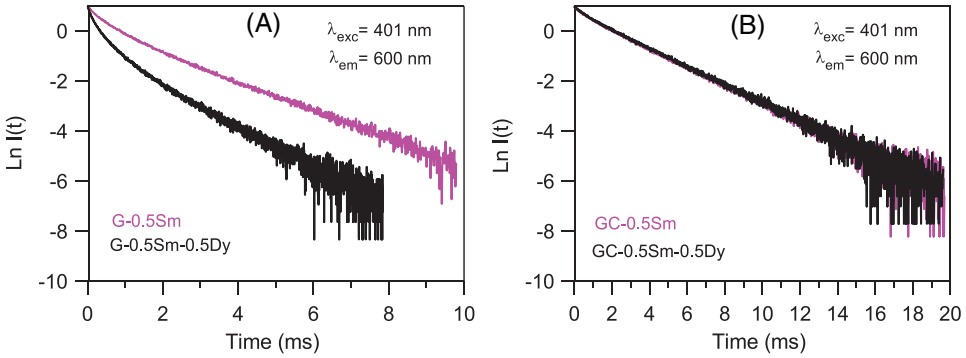

FIGURE 13 Semilogarithmic plot of the fluorescence decays of the $^4G_{5/2}$ level obtained under 401 nm excitation for the single and codoped samples: (A) G-0.5Sm and G-0.5Sm-0.5Dy and (B) GC-0.5Sm and GC-0.5Sm–0.5Dy

energy transfer to Dy^{3+} ions, however the emission and excitation spectra of the codoped samples confirm that there is not any significant energy transfer between Sm^{3+} and Dy^{3+} ions. Therefore, this further reduction of the lifetimes could be due to a decrease of the distance between Sm^{3+} ions due to the addition of Dy^{3+} ions, which increases the interaction between Sm^{3+} ions, and therefore enhance the cross-relaxation processes.

On the other hand, the lifetimes of the $^4G_{5/2}$ level in the codoped glass–ceramic samples (Figure 13B) are practically unaffected by the presence of Dy^{3+} ions. This fact could be due to the lower amount of dopants entering the crystals in the codoped GC samples.

4 | CONCLUSIONS

Glass–ceramics based on Sm^{3+} and Sm^{3+} /Dy^{3+} co-doped $Sr_2MgSi_2O_7$ phosphor have been obtained from sintering and crystallization of glass powders. The relative density of the glass–ceramics is in the range 0.90–0.98. Both, the base glasses and the corresponding glass–ceramics, show red emissions under 401 nm excitation.

Akermanite is the main crystalline phase present in all the glass–ceramic samples. The increase in samarium concentration has a remarkable influence on crystal growth. The crystal size increases from 0.4 μm in the undoped glass–ceramic to 4.5 μm in the glass–ceramic with higher dopant concentration. In addition, the amount of samarium entering the crystals increases with the increase of samarium concentration, but it is reduced with the addition of dysprosium as a codopant, because it is also incorporated inside the crystals as confirmed by EDX analysis. The amount of Sm^{3+} within the crystals is detectable by EDX analysis from the composition with 0.3 mol%, where the crystals have an average size of around 2 μm.

Room-temperature emission spectra of Sm^{3+} ions of the glass and glass–ceramic samples were obtained in the range 525–750 nm after excitation at 401 nm. The emission peaks remain unchanged for all Sm^{3+} concentrations, while the emission intensity increases with increasing concentration up to 0.3 mol% and then decreases due to the presence of nonradiative processes. The presence of nonradiative processes is also reflected by the shortening of the lifetimes and the deviation of the decays from a single exponential function. The emission spectra in the glass–ceramics show a more resolved structure and higher intensity compared to the glass samples, suggesting a different, more crystalline environment for the Sm^{3+} ions. The emission and excitation spectra of the co-doped samples do not reveal significant energy transfer between Sm^{3+} and Dy^{3+} ions. The emission color could be tuned by using different excitation wavelengths in the co-doped glasses. The studied glass–ceramics can be applied as enamels on metallic or ceramic substrates and may be promising materials for photonic devices operating in the visible region.

ACKNOWLEDGMENTS

Funding from MICINN under projects PID2020-115419GB-C-21/C-22/AEI/ 10.13039/501100011033, PID2019-107439GB-I00 and PIE-CSIC 201960E016 is acknowledged.

ORCID

Laura Fernández-Rodríguez https://orcid.org/0000-0001-5789-2423
Rolindes Balda https://orcid.org/0000-0001-6882-3167
Joaquín Fernández https://orcid.org/0000-0003-4673-167X
Alicia Durán https://orcid.org/0000-0002-0067-1934
María Jesús Pascual https://orcid.org/0000-0002-6833-9663

20411294, 2023, 1, Downloaded from https://ceramics.onlinelibrary.wiley.com/doi/10.1111/ijag.16584 by Universidad Del Pais Vasco, Wiley Online Library on [09/02/2023]. See the Terms and Conditions (https://onlinelibrary.wiley.com/terms-and-conditions) on Wiley Online Library for rules of use; OA articles are governed by the applicable Creative Commons License

REFERENCES

1. Hai O, Jiang H, Zhang Q, Ren Q, Wu X, Hu J. Effect of cooling rate on the microstructure and luminescence properties of $Sr_2MgSi_2O_7$: Eu^{2+}, Dy^{3+} materials. Luminescence. 2017;32:1–6. https://doi.org/10.1002/bio.3343
2. Fei Q, Chang C, Mao D. Luminescent properties of $Sr_2MgSi_2O_7$ and $Ca_2MgSi_2O_7$ long lasting phosphors activated by Eu^{2+}, Dy^{3+}. J Alloys Compd. 2005;390:133–7. https://doi.org/10.1016/j.jallcom.2004.06.096
3. Fernández-Rodríguez L, Levy D, Zayat M, Jimínez J, MAther GC, Durán A et al. Processing and luminescence of Eu/Dy-doped $Sr_2MgSi_2O_7$ glass–ceramics. J Eur Ceram Soc. 2021;41:811–22. https://doi.org/10.1016/j.jeurceramsoc.2020.08.038
4. Xu J, Tanabe S. Persistent luminescence instead of phosphorescence: History, mechanism, and perspective. J Lumin. 2019;205:581–620. https://doi.org/10.1016/j.jlumin.2018.09.047
5. Mahamuda S, Swapna K, Venkateswarlu M, Srinivasa Rao A, Shakya S, Vijaya Prakash G. Spectral characterisation of Sm^{3+} ions doped Oxy-fluoroborate glasses for visible orange luminescent applications. J Lumin. 2014;154:410–24. https://doi.org/10.1016/j.jlumin.2014.05.017
6. Sharma YK, Surana SSL, Singh RK. Spectroscopic investigations and luminescence spectra of Sm^{3+} doped soda lime silicate glasses. J Rare Earths. 2009;27:773–80. https://doi.org/10.1016/S1002-0721(08)60333-6
7. Kiran N, Baker AP, Wang GG. Synthesis and luminescence properties of MgO:Sm^{3+} phosphor for white light-emitting diodes. J Mol Struct. 2017;1129:211–5. https://doi.org/10.1016/j.molstruc.2016.09.046
8. Wang L, Noh H, Moon B, Choi B, Jeong J, Shi J. Luminescent properties and energy transfer of Sm^{3+} doped $Sr_2CaMo_{1-x}W_xO_6$ as a potential phosphor for white LEDs. J Alloys Compd. 2016;663:808–17. https://doi.org/10.1016/j.jallcom.2015.12.179
9. Li Q, Noh H, Moon B, Choi B, Jeong J, Shi J. The origin of efficiency enhancement of inorganic/organic hybrid solar cells by robust samarium phosphate nanophosphors. Sol Energy Mater Sol Cells. 2014;130:426–34. https://doi.org/10.1016/j.solmat.2014.07.033
10. Suhasini T, Kumar J, Sasikala T, Jang K, Sueb H, Jayasimhadri M, et al. Absorption and fluorescence properties of Sm^{3+} ions in fluoride containing phosphate glasses. Opt Mater (Amst). 2009;31:1167–72. https://doi.org/10.1016/j.optmat.2008.12.008
11. Shoaib M, Rooh G, Rajaramakrishna R, Chanthima N, Kim HJ, Tuscharoen S, et al. Physical and luminescence properties of samarium doped oxide and oxyfluoride phosphate glasses. Mater Chem Phys. 2019;229:514–22. https://doi.org/10.1016/j.matchemphys.2019.03.016
12. Chen C, Yu C, Xu F, Li Q, Zhang Y. High energy transfer in Dy^{3+} /Sm^{3+}co-doped transparent borosilicate glass–ceramics containing novel $Na_5Y_9F_{32}$ nanocrystals for w-LEDs applications. Ceram Int. 2021;47:1–9. https://doi.org/10.1016/j.ceramint.2020.08.190
13. Zhang L, He F, Xie J, Liu J. Structure and luminescent properties of Sm^{3+} doped SrO–MgO–SiO_2 glass ceramics. J Wuhan Univ Technol Sci Ed. 2015;30:282–7. https://doi.org/10.1007/s11595-015-1140-7
14. Online VA, Wondraczek L, Krolikowski S, Nass P. Europium partitioning, luminescence re-absorption and quantum efficiency in (Sr,Ca) akermanite–feldspar bi-phasic glass ceramics. J Mater Chem C. 2013;4078:4086. https://doi.org/10.1039/c3tc30609g
15. Pascual MJ, Pascual L, Durán A. Determination of the viscosity–temperature curve for glasses on the basis of fixed viscosity points determined by hot stage microscopy. Phys Chem Glass. 2001;42:61–6.
16. Pascual MJ, Duran A. A new method for determining fixed viscosity points of glasses. Phys Chem Glass. 2005;46:512–20.
17. Zaid MHM, Sidek HAA, El-Mallawany R, Almasri KA, Matori KA. Synthesis and characterization of samarium doped calcium soda-lime-silicate glass derived wollastonite glass–ceramics. J Mater Res Technol. 2020;9:13153–60. https://doi.org/10.1016/j.jmrt.2020.09.058
18. Seshadri M, Radha M, Rajesh D, Barbosa LC, Cordeiro CMB, Ratnakaram YC. Effect of ZnO on spectroscopic properties of Sm^{3+} doped zinc phosphate glasses. Phys B: Condens Matter. 2015;459:79–87. https://doi.org/10.1016/j.physb.2014.11.016
19. Reisfeld R. Spectra and energy transfer of rare earths in inorganic glasses. Rare Earths: Structure and Bonding, Berlin: Springer; 1973;13:53–98. https://doi.org/10.1007/3-540-06125-8_2
20. Ramteke DD, Kumar V, Swart HC. Spectroscopic studies of Sm^{3+}/Dy^{3+} co-doped lithium boro-silicate glasses. J Non Cryst Solids. 2016;438:49–58. https://doi.org/10.1016/j.jnoncrysol.2016.02.010
21. Li X, Wang X, Li X, Cheng L, Tong L, Wang W et al. Luminescence studies of Sm^{3+} single-doped and Sm^{3+}, Dy^{3+} co-doped $NaGdTiO_4$ phosphors. Phys B Condens Matter. 2016;481:197–203. https://doi.org/10.1016/j.physb.2015.11.017
22. Kesavulu CR, Jayasankar CK. Spectroscopic properties of Sm^{3+} ions in lead fluorophosphate glasses. J Lumin. 2012;132:2802–9. https://doi.org/10.1016/j.jlumin.2012.05.031

How to cite this article: Fernández-Rodríguez L, Balda R, Fernández J, Durán A, Pascual MJ. Structure and luminescent properties of Sm/Dy-doped $Sr_2MgSi_2O_7$ glass–ceramics. Int J Appl Glass Sci. 2023;14:140–154. https://doi.org/10.1111/ijag.16584

20411294, 2023, 1, Downloaded from https://ceramics.onlinelibrary.wiley.com/doi/10.1111/ijag.16584 by Universidad Del Pais Vasco, Wiley Online Library on [09/02/2023]. See the Terms and Conditions (https://onlinelibrary.wiley.com/terms-and-conditions) on Wiley Online Library for rules of use; OA articles are governed by the applicable Creative Commons License